Geophys. J. Int. (1997) **130,** 167–182

Mantle structure beneath Indonesia inferred from high-resolution tomographic imaging

Sri Widiyantoro[1,*] and Rob van der Hilst[2]

[1] *Research School of Earth Sciences, Australian National University, Canberra,* ACT 0200, *Australia*
[2] *Department of Earth, Atmospheric, and Planetary Sciences, Massachusetts Institute of Technology, Cambridge,* MA 02139–4307, *USA*

Accepted 1997 March 6. Received 1997 March 3; in original form 1996 September 13

SUMMARY

We investigated mantle structure beneath the Indonesian region by means of tomographic inversions of traveltime residuals of direct *P* and the surface-reflected depth phases *pP* and *pwP*. The hypocentres and phase data used in the inversions were derived from the reprocessing of data reported to international data centres, which include data from the Australian SKIPPY project. We used more than 6.0×10^6 data from more than 50 000 globally distributed earthquakes recorded at a subset of nearly 3000 seismological stations worldwide. The use of depth phases improved the sampling of the upper-mantle structure, in particular beneath the back-arc regions. The mapping of distant aspherical mantle structure into the study region was minimized by combining a high-resolution regional with a low-resolution global inversion. The inversion was linearized around the ak135 reference velocity model, and a combination of minimum norm and gradient damping was applied to constrain the solution. Inversion of different subsets of the data and test inversions of synthetic data indicate that resolution is sufficient to substantiate the conclusions pertinent to the complex large-scale structure of the subducted slab beneath the Indonesian archipelago.

The tomographic images confirm previous evidence for regional slab penetration into the upper part of the lower mantle but suggest a more complex trajectory of mantle flow beneath Indonesia. The implied lateral variation in the shape of the upper-mantle slab is generally in good agreement with inferences from seismicity. The data reveal a seismic anomaly beneath the Sunda arc, which is detected to at least 1500 km in depth and forms the eastern end of a deep anomaly associated with the past subduction of lithosphere of the Mesozoic Tethys ocean. Below Java the lithospheric slab is probably continuous from the Earth's surface to the lower mantle, but beneath Sumatra the deep slab seems to be detached from the seismogenic slab. The high-resolution images suggest that the subducted slab is deflected in the transition zone beneath the Banda arc and that the descending slabs form a spoon-shaped structure. North of the Banda Sea we detect the two opposing subducted slabs of the Molucca Sea plate; this is consistent with previous studies, but our images suggest that the westward subduction has a significantly steeper dip than the eastward subduction. Slab structure beneath the Banda and Molucca seas is explained in the context of the continent–arc collision between Australia and the southeast Indonesian Island arc, and the arc–arc collision between Sangihe and Halmahera. Inversion of traveltime residuals of direct *S* phases, a novelty for this region, largely confirms the inferences from the *P*-wave data, even though less detail is resolved.

Key words: body waves, Indonesia, mantle, seismic tomography.

1 INTRODUCTION

The tectonic setting of the Indonesian archipelago in southeastern Eurasia is determined by the complex interaction of several major and minor plates (Fig. 1). The junction of island arcs includes the Sunda arc, the Banda arc, the Sangihe arc to the west of the Molucca collision zone (MCZ) and the Halmahera arc to the east. The Sunda arc, from northwestern Sumatra to Flores, marks the subduction of the Indo-Australian plate beneath the Eurasian plate. The Banda arc to the east of the Sunda arc displays a strong curve in map view.

---

[*] On leave from: Department of Geophysics and Meteorology, Bandung Institute of Technology, Bandung 40132, Indonesia.

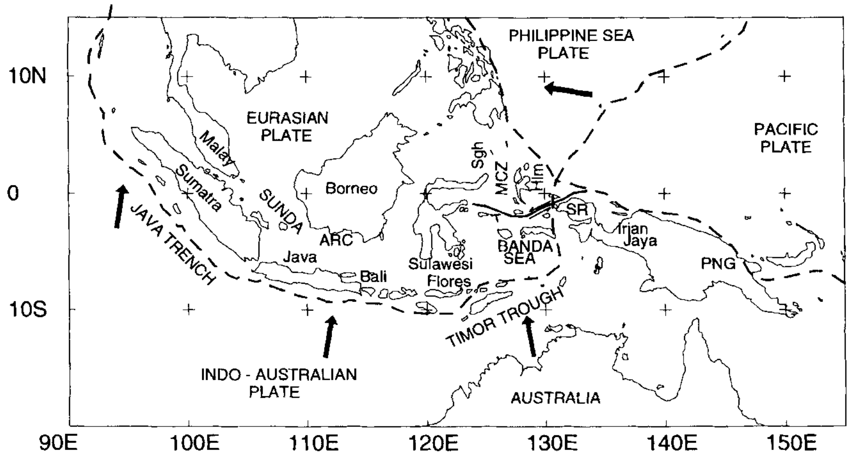

Figure 1. Map of the study region. Dashed lines indicate major plate boundaries after NUVEL-1, DeMets *et al.* (1990). The solid line to the north of the Banda Sea depicts the Sorong fault. Arrows indicate the direction of plate motion relative to the Eurasian plate. Abbreviations used: MCZ, Molucca collision zone; PNG, Papua New Guinea; SR, Sorong; Hlm, Halmahera; Sgh, Sangihe.

The strike of the Banda arc used to be east–west, just like the eastern part of the Sunda arc, but it was twisted counter-clockwise in the Pliocene due to the combination of the collision with the northward-moving Australian continent, the counter-clockwise rotation of New Guinea, and the westward thrust along the Sorong fault system. These tectonic events interrupted the regular growth of the eastern Indonesian arc (Katili 1975). The Sorong fault, striking nearly east–west from the Bird's Head of Irian Jaya to the east of central Sulawesi, marks the boundary between Banda and Halmahera. The active collision between Halmahera and Sangihe, the only known example of two colliding arcs, has caused the two opposing subduction directions of the Molucca Sea plate (Hamilton 1979; Cardwell, Isacks & Karig 1980; Hall 1987).

The convergence rate of the Indo–Australian and Eurasian plates increases from about 60 mm yr^{-1} near Sumatra to 78 mm yr^{-1} in the easternmost part of the Sunda arc, with an azimuth N20°E predicted by the RM2 plate model (Minster & Jordan 1978). A recent study based on the first geodetic measurement of convergence across the Java trench (Tregoning *et al.* 1994) suggests that convergence of 67 ± 7 mm yr^{-1} is measured between Christmas Island, southwest of Java, and west Java in a direction of N11°E ± 4°. This is similar to the relative plate velocity of 71 ± 2 mm yr^{-1} between Australia and Eurasia according to NUVEL-1 (DeMets *et al.* 1990). In the east, the slip rate increases from ~ 80 mm yr^{-1} near the Philippines to ~ 100 mm yr^{-1} near Halmahera (Ranken, Cardwell & Karig 1984). The age of the subducted oceanic lithosphere increases eastwards from about 50–90 Myr below Sumatra to 140–160 Myr near Flores. The age of the Molucca Sea lithosphere, however, is unknown.

Given this tectonic setting, it can be expected that the junction of island arcs overlies a strongly heterogeneous mantle. This structural complexity is partly evident from regional seismicity. The character of subduction-related seismicity changes abruptly from Sumatra to Java. With the exception of some small events in the southeast, seismicity does not exceed a depth of about 300 km beneath Sumatra, but earthquakes occur at depths of up to 670 km below Java, Banda and Sangihe. A pronounced seismic gap exists below Java in a depth interval of about 300–500 km (e.g. Newcomb & McCann 1987; Wortel & Vlaar 1988). The Wadati–Benioff zone is steep below Java and dips rather gently beneath the easternmost Banda arc. Beneath the MCZ, Wadati–Benioff zones dip to the west and to the east below Sangihe and Halmahera, respectively (Cardwell *et al.* 1980).

The aim of this study is to explore the deep structure of slabs beneath the region by means of tomographic imaging. Until the late 1980s investigations of mantle structure beneath the Indonesian region were mostly based on volcanism, marine geophysical data and seismicity (e.g. Katili 1975; Cardwell & Isacks 1978; Hamilton 1979; Hall 1987), and lower-mantle structure had not yet been revealed. Previous seismic tomographic studies of mantle structure below the region were undertaken by Fukao *et al.* 1992 and Puspito *et al.* 1993. Fukao *et al.* (1992) argued that the slab beneath the eastern Sunda arc penetrates directly into the lower mantle, where it deflects in the uppermost lower mantle and sinks vertically to a depth of at least 1200 km. Puspito *et al.* (1993) also detected slab penetration to the lower mantle beneath Java and, in addition, presented evidence for two opposing subducted slabs of the Molucca Sea plate. These tomographic studies did not use depth phases such as *pP* and *pwP*. In this study we included those depth phases in order to improve the sampling of structure, especially in the upper mantle beneath the back-arc regions, and to constrain earthquake focal depths (Van der Hilst *et al.* 1991; Van der Hilst & Engdahl 1991, 1992). Following Fukao *et al.* (1992), we incorporated a global inversion in this regional study to minimize the mapping of signals from structures outside the study region. Our results are generally in good agreement with the results of previous studies, but reveal the structural complexity in more detail, in particular in the upper mantle and transition zone.

We also inverted traveltime residuals of *S* phases to investigate the differences from and the similarities with the structure as revealed by the inversion of *P* data, which can help to provide a better understanding of the physical origin of the wave-speed anomalies. Routinely processed *S* data are generally regarded to be more noisy than *P* data. For *P* and also for *S* we used the carefully reprocessed data set of Engdahl, Van der Hilst & Buland (1997). The *S* residuals have larger uncertainties than the *P* data but thanks to the reprocessing they do not have some of the problems inherent in ISC *S* data. In contrast to ISC procedures, Engdahl *et al.* (1997) used *S* phases in the initial source location and a reference velocity model (ak135 of Kennett, Engdahl & Buland 1995) that is more appropriate for *S* than the reference model used by the ISC.

In a previous paper (Widiyantoro & Van der Hilst 1996), hereinafter referred to as INA1, we focussed on the complex structure beneath the Sunda arc. In this paper we briefly summarize the structure beneath the Sunda arc and present results of the comprehensive resolution tests used to substantiate the arguments in INA1. In addition, we discuss the structure beneath the Banda, MCZ, and Philippine Island regions as inferred from the tomographic images, and present some results of the inversion of *S* data.

2 METHOD

In this section we describe the tomographic method used, including the model parametrization used for regional and global inversions, the system of linear equations and the resolution tests used to assess image quality.

2.1 Model parametrization

We discretized the entire mantle by means of local basis functions in the form of a uniform grid of constant velocity cells of 5° × 5°, but in the study area we used a finer grid of 1° × 1° in order to allow the resolution of relatively small-scale structure (Fig. 2a). The cell layer divisions inside and outside the volume under study are displayed in Fig. 2(b). We discretized the mantle volume under study, to a depth of 1600 km, into 19 layers with layer thicknesses ranging from 35 km in the uppermost layer to 200 km for the layer centred at 1500 km. For the global inversion, we used 16 layers with an average layer thickness of about 180 km (Table 1). The number of small and big cells is 43 225 and 41 472, respectively.

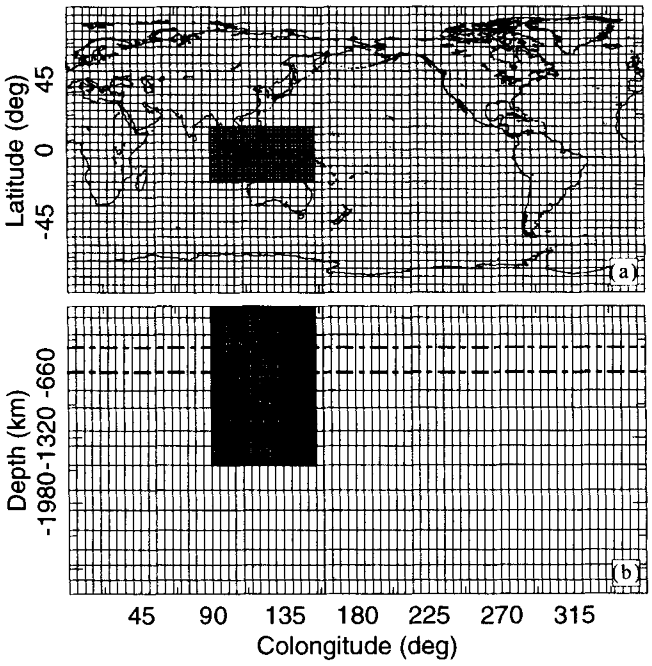

Figure 2. Model parametrization. (a) The grid of non-overlapping blocks of horizontal dimension of 1° × 1° and 5° × 5° depicts the parametrization used inside and outside the study region, respectively. (b) Cell layer divisions inside and outside the study region; the *y*-axis is exaggerated seven times.

On inversion we also accounted for the effect on the travel-time residuals of source mislocation due to 3-D structure. Instead of solving for four relocation parameters for each earthquake we used the same partial derivatives for all earthquakes located within an event cluster. This reduced the number of unknowns considerably. We used 5916 event clusters with a dimension of 1° × 1° × 50 km, adding almost 23 664 parameters (eq. 3) to the 84 697 unknowns associated with the constant-slowness blocks. The total number of unknowns to be solved for by the tomographic inversion is thus almost 110 000.

For stations and/or events located outside the mantle volume under study we combined ray paths from event to station clusters into a single 'summary' ray (INA1). This suppresses noise, reduces the uneven sampling of mantle structure by ray paths, and decreases the demands on computer memory, mass storage and cpu time. The datum (residual time) assigned to

Table 1. Information of the cell layer division *inside* and *outside* the volume under study, and the corresponding layer-average velocity of the ak135 model (Kennett *et al.* 1995).

Layer no.	Depth range (km)	Average velocity (km/s)
Inside:		
1	0–35	6.10
2	35–70	8.04
3	70–110	8.05
4	110–160	8.10
5	160–220	8.25
6	220–280	8.45
7	280–340	8.67
8	340–410	8.90
9	410–490	9.49
10	490–570	9.76
11	570–660	10.05
12	660–750	10.91
13	750–840	11.12
14	840–930	11.28
15	930–1020	11.42
16	1020–1130	11.58
17	1130–1250	11.76
18	1250–1400	11.95
19	1400–1600	12.18
Outside:		
1	0–110	7.43
2	110–280	8.27
3	280–410	8.80
4	410–660	9.78
5	660–840	11.01
6	840–1020	11.35
7	1020–1250	11.67
8	1250–1400	11.95
9	1400–1600	12.18
10	1600–1850	12.47
11	1850–2050	12.74
12	2050–2250	12.97
13	2250–2450	13.20
14	2450–2600	13.40
15	2600–2750	13.58
16	2750–2889	13.67

the summary ray is the median of all data considered for that summary ray. There is no restriction on the number of rays that contribute to a summary ray.

2.2 Tomographic system of equations

In regional tomographic studies one usually considers only a fraction of the whole Earth's mantle volume and sets up the following system of linear equations for least-squares inversion:

$$\mathbf{A}\mathbf{x} = (\mathbf{L}_{\mathrm{in}}/\mathbf{S}_{\mathrm{a}}/\mathbf{R})\begin{pmatrix}\mathbf{s}_{\mathrm{in}}\\ \mathbf{s}_{\mathrm{a}}\\ \mathbf{r}\end{pmatrix} = \delta\mathbf{t}, \tag{1}$$

where matrix $\mathbf{A}$ consists of the matrices $\mathbf{L}_{\mathrm{in}}$, $\mathbf{S}_{\mathrm{a}}$ and $\mathbf{R}$ containing ray-segment lengths in cells in the study region, station correction coefficients and event relocation coefficients, respectively. Model vector $\mathbf{x}$ contains the corresponding solution vectors $\mathbf{s}_{\mathrm{in}}$, $\mathbf{s}_{\mathrm{a}}$ and $\mathbf{r}$ and is projected by $\mathbf{A}$ on the data vector $\delta\mathbf{t}$ of traveltime residuals. In this study we inverted simultaneously for global structure and replaced $\mathbf{S}_{\mathrm{a}}$ by the matrix $\mathbf{L}_{\mathrm{out}}$, whose elements represent the total length of rays in each of the large cells outside the region of our particular interest:

$$(\mathbf{L}_{\mathrm{in}}/\mathbf{L}_{\mathrm{out}}/\mathbf{R})\begin{pmatrix}\mathbf{s}_{\mathrm{in}}\\ \mathbf{s}_{\mathrm{out}}\\ \mathbf{r}\end{pmatrix} = \delta\mathbf{t}. \tag{2}$$

Here, $\mathbf{s}_{\mathrm{in}}$ and $\mathbf{s}_{\mathrm{out}}$ are the slowness perturbations inside and outside the volume under study, and $\mathbf{r}$ is the event relocation solution vector. Eq. (2) shows that the inversion allows for the simultaneous determination of velocity perturbations in the study area and the whole mantle, and event relocation upon inversion. Test inversions based on either (1) or (2) suggest that the two methods give similar results.

To compute $\mathbf{L}_{\mathrm{in}}$ and $\mathbf{L}_{\mathrm{out}}$ for the construction of matrix $\mathbf{A}$ we traced seismic rays through a radially stratified medium represented by Mohorovičić's law (*cf.* Bullen & Bolt 1985), which provides a good approximation to the actual velocity variation over many depth ranges in the Earth. For source relocation we used the partial derivatives given by Gubbins (1990):

$$dT_{ij} = (\partial T_{ij}/\partial t_{o,i})dt_{o,i} + (\partial T_{ij}/\partial h_i)dh_i + (\partial T_{ij}/\partial \theta_i)d\theta_i + (\partial T_{ij}/\partial \phi_i)d\phi_i, \tag{3}$$

with

$$\partial T_{ij}/\partial t_{o,i} = 1.0, \tag{3a}$$

$$\partial T_{ij}/\partial h_i = -(\eta_i^2 - p_{ij}^2)^{1/2}/r_i, \tag{3b}$$

$$\partial T_{ij}/\partial \theta_i = -p_{ij}\cos Z_{ij}, \tag{3c}$$

$$\partial T_{ij}/\partial \phi_i = p_{ij}\sin Z_{ij}\sin\theta_i, \tag{3d}$$

and T_{ij} the traveltime for event i and station j, $t_{o,i}$ the origin time, h_i the focal depth, (θ_i, ϕ_i) the colatitude and colongitude of the epicentre, r_i the radius from the Earth's centre to the hypocentre, p_{ij} the ray parameter, Z_{ij} the azimuth, $\eta_i = r_i/v(r_i)$, and $v(r_i)$ the velocity as a function of radius. The velocity $v(r_i)$ is taken from the reference velocity model used, and p_{ij}, Z_{ij} and θ_i are provided in the data set of Engdahl *et al.* (1997).

To solve (2) for $\mathbf{x}$ we used the iterative LSQR method of Paige & Saunders (1982), a conjugate gradient technique first applied to seismic tomography by Nolet (1985). On inversion we used two kinds of explicit damping: the first damping (minimum norm) biases towards zero slowness perturbations from an average model and suppresses the amplitude in regions of poor sampling (Spakman & Nolet 1988); the application of the second (gradient) damping, which biases toward a smooth model, is conducted using a roughening matrix described by Nolet (1987). Application of the gradient damping results in a relatively smooth model that facilitates its use as input for quantitative geodynamical studies, for instance the investigation of the lateral strength of slabs (Moresi & Gurnis 1996). The gradient damping was applied separately to the blocks inside and outside the study area to avoid smoothing from the low- into the high-resolution part of the model.

We tuned the inversion carefully in order to obtain good results both inside and outside the study area since better constraints on anomalies elsewhere minimize smearing into the study region. Therefore, we actually performed the global inversion with all available data and thus also considered paths that did not transect the mantle volume under study. In Fig. 3, we present an example of a velocity-perturbation map for a global layer in the upper mantle. It reveals a pronounced low P-wave-speed region around the Pacific, consistent with results of previous global studies, e.g. Inoue *et al.* (1990), and regions of high P wave speed associated with cratonic parts of the continents. For instance, the global images display the sharp contrast between high and low wave speeds across the Tornquist–Teissyre Zone in Europe (Zielhuis & Nolet 1994), and suggest that this contrast extends southeastwards all the way to India. It also demonstrates the significant difference between the image resolution inside and outside the study region. For example, the high-wave-speed anomaly, in the bottom right corner of the study region, associated with the oceanic lithosphere of the Coral Sea, and the slab along the Indonesian Island arc are well imaged; these structures would have been smoothed out in models based on a coarser parametrization.

2.3 Resolution tests

We assessed the tomographic images by conducting inversions of synthetic data computed from artificial but known 3-D models using the same ray coverage and linearized theory as used in the real data inversion. We also used different subsets of data, for example different time periods and focal depth intervals, to test the sensitivity of the model to differences in data coverage. Among the techniques most often used are sensitivity tests (Spakman & Nolet 1988; Humphreys & Clayton 1988) and checker-board tests (Inoue *et al.* 1990; Fukao *et al.* 1992). The techniques, however, have limitations (Van der Hilst, Engdahl & Spakman 1993; Léveque, Rivera & Wittlinger 1993) that may lead to incorrect assessment of the reliability of tomographic images. Léveque *et al.* (1993) argued that the inferences pertinent to image quality depend on the spatial characteristics of the input model used to compute the synthetic data. In addition, we realize that the tests with synthetic data do not simulate accurately the effect of source mislocation and errors in the data and that they are conducted with the same approximations (e.g. model parametrization) and theoretical assumptions (e.g. linearization and the neglect of anisotropy) as in the inversion of the real data phase.

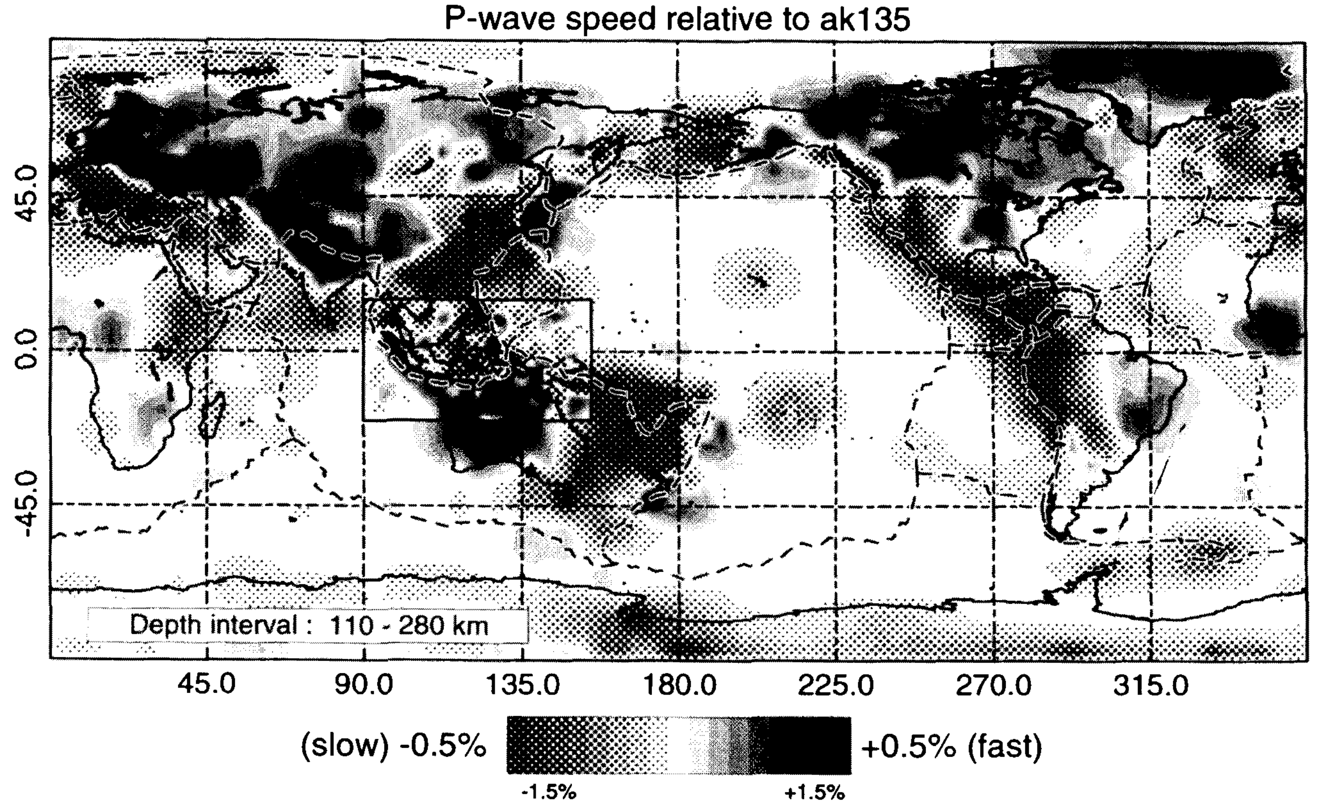

Figure 3. Layer anomaly map depicting results of the inversion for upper-mantle structure. Contour scales are −1.5 to +1.5 per cent and −0.5 to +0.5 per cent relative to ak135 for solutions inside and outside the study area, respectively.

In assessing the solution quality, we have conducted some checker-board and target anomaly tests. In this paper, however, our main purpose is to assess the resolution of major (large-scale) slab structure beneath the study region. Therefore, we choose to present the results of hypothesis testing using input models that have similar spatial characteristics to the slab structure inferred from the real data inversion. One of the advantages of this approach is that the effects of regularization on the images are similar to that in the inversion of the reported data. We computed the synthetic data by taking the difference between traveltimes calculated in a 3-D input model (for example a slab model or a checker-board pattern) and in the 1-D reference model used. To simulate errors in the data, we added random artificial errors to the synthetic data between −1.0 and +1.0 s for *P*, and between −1.5 and +1.5 s for *pP* and *pwP*. We inverted the noisy synthetic data using damping parameters used in the real data inversion to see how well the shape of the input model and the amplitude are recovered. Judging from the recovery, we can tune the inversion by exploring the damping parameters that give the optimum trade-off between bias (that is the amplitude recovery and smoothness in the model) and the variance reduction of the data. In Section 4 we present in horizontal and vertical slices the results of hypothesis testing, along with the real data inversion.

3 DATA

The data used in this study are traveltime residuals produced by event relocation and phase re-identification based on arrival times reported to the International Seismological Centre (ISC) from 1964 to 1992, and to the National Earthquake Information Center (NEIC) from 1993 to 1995 (Engdahl *et al.* 1997). This data set includes data from about 40 portable seismographs deployed in the Australian SKIPPY project (Van der Hilst *et al.* 1994). Engdahl *et al.* (1997) used an improved global traveltime model ak135 (Kennett *et al.* 1995) and arrival times of first-arriving regional and teleseismic *P* phases, regional *S* phases, depth phases (*pP*, *pwP* and *sP*) and the *PKPdf* branch to relocate all teleseismically well-constrained earthquakes that have occurred during the period 1964–1995. Their procedure ensures that depth errors and the mapping of source heterogeneity into mislocation are minimized, and it creates a powerful uncontaminated database of *P*, *pP* and *pwP* residuals for use in tomographic inversions. Hereafter, the reprocessed data used in this study are referred to as EVB data. We used almost 17 000 (35 000) events inside (outside) the volume under study, recorded at a subset of almost 3000 stations worldwide (Figs 4a & b). All epicentral distances are considered. We used more than 6.0×10^6 data for the construction of summary rays (see Section 2.1). For the inversion we only kept the summary rays for which the absolute traveltime residual has a magnitude less than 5.0 s. If both the source and receiver were located within the study region we used individual ray paths to optimize the sampling. The total number of paths and traveltime residuals constituting the linear system is nearly 550 000.

Fig. 5 depicts the distribution of the stations and earthquake epicentres used in this study and the *pP&pwP* surface reflection points inside the study area. The region between Java and

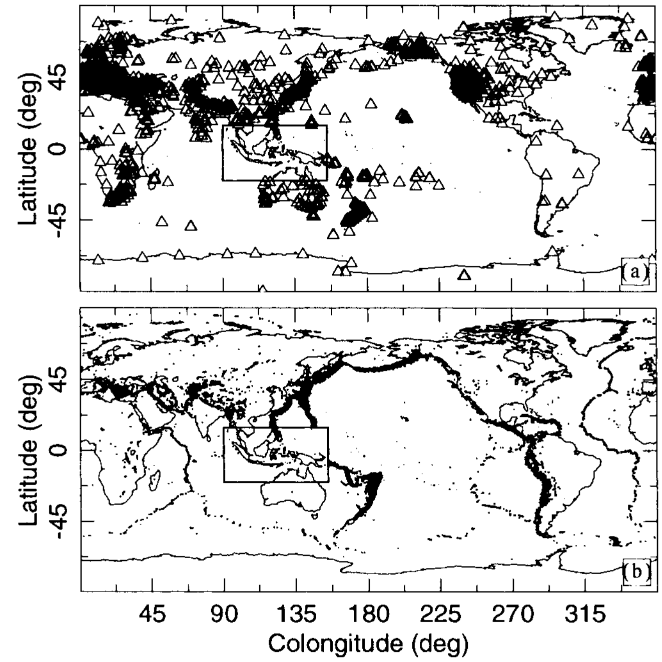

Figure 4. Distribution of stations and epicentres outside the study area. (a) Open triangles depict stations; (b) small dots depict epicentres of earthquakes.

Borneo with only few reflection points (Fig. 5c) reflects the pronounced seismic gap between depths of 300 and 500 km beneath the eastern Sunda arc. Comparison of the sampling by either *P*-wave paths or the combination of *P&pP&pwP* paths (Fig. 6) demonstrates that for regions away from the trench, e.g. south Borneo, and the area between Timor and Australia, sampling is improved through the incorporation of depth phases.

4 PRESENTATION OF TOMOGRAPHIC IMAGES

We interpret *P*-wave traveltime residuals in terms of velocity perturbations relative to the ak135 reference velocity model (Kennett *et al.* 1995). In this section we present the images (achieved after conducting 50 iterations with the LSQR algorithm) for the entire Indonesian region. The variance reduction upon inversion is 31 per cent. Notice that we used the EVB data set, which has a variance that is already significantly smaller than that of published ISC *P* residuals (Van der Hilst *et al.* 1991; Van der Hilst & Engdahl 1992; Engdahl *et al.* 1997). We discuss three anomaly maps for depth intervals representing the upper mantle, the transition zone and the lower mantle.

Anomaly maps for a sequence of depth intervals depict the slab as a region of higher-than-average *P*-wave speed in the mantle (Figs 7a–c). Most parts of the region of interest, in particular along the island arcs, are sufficiently sampled by seismic rays (Figs 7d–f). The image of the slab in the upper mantle (Fig. 7a) resembles the present-day Java trench, Timor trough, the curved Banda arc and the Molucca collision zone. It also reveals fast *P*-wave propagation beneath northern Australia, consistent with a thick continental lithosphere (Zielhuis & Van der Hilst 1996). In the transition zone (Fig. 7b) a high-wave-speed slab is detected beneath the Java and Banda arcs, but not beneath central Sumatra. In the lower mantle (Fig. 7c) the observed prominent and robust feature is the elongate structure of faster-than-average *P*-wave propagation trending E–W over a distance of about 2500 km from below the northwestern tip of Sumatra to below the southern Philippines. Resolution tests demonstrate that these large-scale anomalies are well resolved. In particular, inversions of synthetic data computed from a specifically designed slab model suggest that the shape of major structure is reliably imaged, but the amplitude of the anomalies is underestimated significantly (Figs 7g–i). The observed deep slab beneath Indonesia (Fig. 7c) is confirmed by the result of the inversion of *S* traveltime residuals (Fig. 8a) and is also resolved by the *S* data (Fig. 8b).

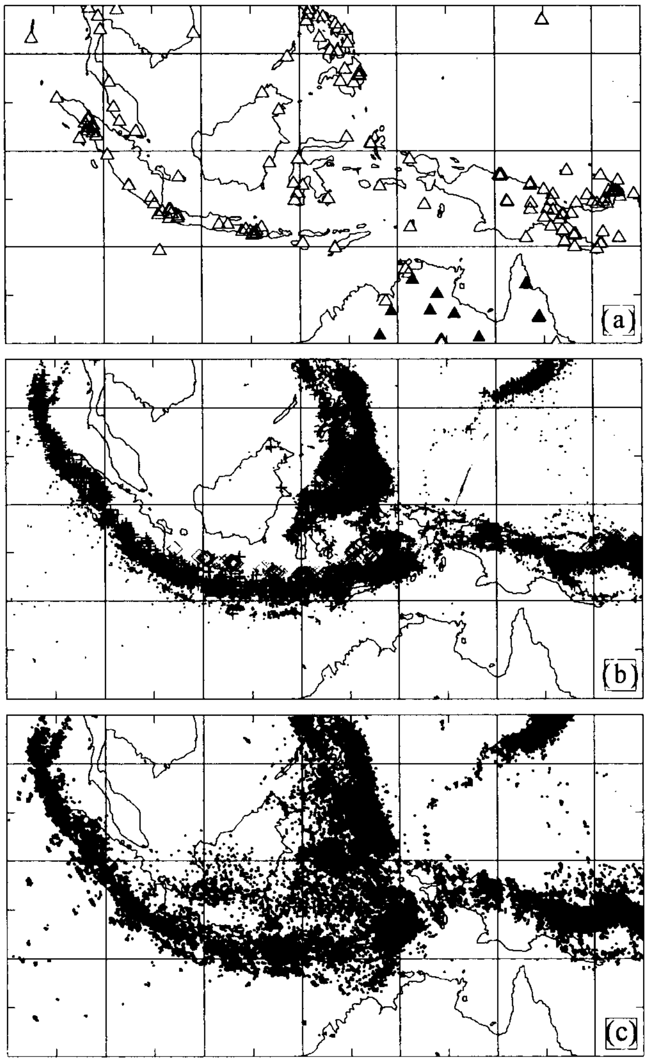

Figure 5. Distribution of stations, epicentres and *pP&pwP* surface reflection points within the study area. (a) Solid triangles depict SKIPPY stations. (b) Epicentre distribution of earthquakes that occurred between 1964 and 1995 in the study region. Locations after ISC (EVB locations). Small dots, crosses and diamonds depict epicentres of shallow ($0 < z \leq 70$ km), intermediate ($70 < z \leq 300$ km) and deep ($z > 300$ km) events, where z is the hypocentre depth. (c) Small dots depict surface reflection points of *pP* and *pwP* waves. The reflection points of *pP* and *pwP* are at land–air or land–water and water–air interfaces, respectively.

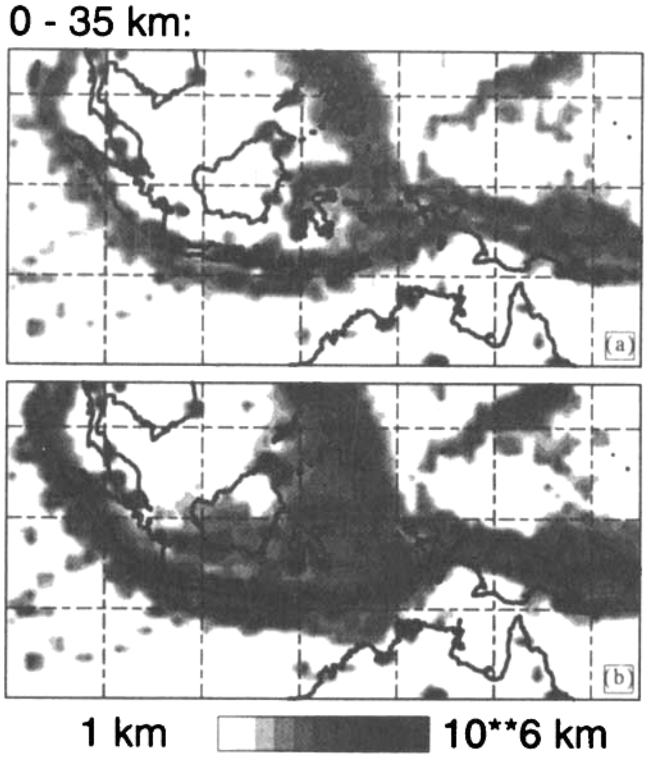

Figure 6. Sampling by seismic rays in the top layer inside the study region. Hereafter, sampling is plotted in logarithmic scale of the total ray length in each block defined by the model parametrization. (a) Sampling by *P* ray only; (b) sampling by *P*, *pP* and *pwP* rays.

In the upper mantle and transition zone the dimension of the smallest feature that is resolved is about 150–200 km. In the lower mantle the resolution length is of the order of about 300–400 km based on *P*-wave imaging. Notice that resolution generally degrades with increasing distance away from the slab due to irregular or poor sampling. With this and the shortcomings of the resolution tests in mind we only interpret the large-scale structures. In the following we focus on the three regions indicated by the three boxes shown in Fig. 9.

4.1 The Sunda arc

In accord with previous studies, the lithospheric slab is imaged as a feature stretching from the surface to the lower mantle below the eastern Sunda arc with a local deflection where the slab continues into the lower mantle. However, our images suggest that the deep slab is detached from the seismogenic slab beneath Sumatra (INA1) and perhaps beneath Java as well.

Three vertical sections across the Sunda arc are repeated from INA1 to illustrate the inferred lateral variation in slab morphology along the arc (Figs 10a–c). Here, we address the resolution of the inferred slab detachment beneath Sumatra and the 'necking' of the slab beneath the eastern Sunda arc using semi-realistic 3-D slab models. We used two slab models: one with a continuous and one with a detached slab. The recovery of the continuous slab suggests that our inversion would be able to resolve such a continuous feature. Here, we only present the model of the detached slab (Figs 10d–f). We added low-wave-speed anomalies adjacent to the model slab in order to investigate the possibility that horizontal smearing of such low-velocity anomalies gives the appearance of slab detachment. The recovery is given in Figs 10(g)–(i). Notice, in particular, that the low-velocity anomalies do not interact to conceal the fast slab. On the contrary, some low-amplitude smearing occurs in the down-dip direction, which may indicate that the gap in which the slab seems absent is even larger than inferred from the images.

As for the Java slab, the resolution test results indicate that sampling is possibly sufficient to discriminate between a continuous and a detached slab but the recovery does reveal significant smearing in the down-dip direction (Figs 10h and i). The images suggest the presence of a thinner slab (perhaps due to 'necking') across the pronounced seismic gap (Figs 10b and c), but this interpretation is necessarily tentative for such detail is probably at the edge of our current resolution. The tests suggest that the kink in the slab is well resolved.

4.2 The Banda arc

Despite numerous studies of the Banda region, e.g. Cardwell & Isacks (1978), Hamilton (1979), Von der Borch (1979) and McCaffrey (1988), there is no consensus on the complicated structure beneath the Banda region. Cardwell & Isacks (1978) investigated the geometry of the subducted lithosphere in the upper mantle and transition zone beneath the Banda Sea from seismicity and fault-plane solutions. Their conclusions are confirmed by our current study.

The inversion reveals the twisting of the slab in the upper mantle, which parallels the present-day curved Banda arc (Fig. 11a). Resolution tests indicate that sampling by seismic rays is sufficient to recover slab structure beneath the Banda region, in particular along the arc (Figs 11b and c). At this depth interval (110–160 km), the twisted slab seems to connect with the top of the two opposing subducted slab associated with the Molucca Sea plate. The lateral variation in slab structure beneath the region is further illustrated by vertical sections across the arc (Figs 12a and b). Resolution tests (Figs 12c–f) reveal that the northward- and westward-subducting slabs are resolved. The observed anomaly, which stretches in an E–W direction just beneath the 660 km discontinuity (Fig. 12b), is, technically speaking, within the resolving power of the data used. Beneath the westernmost part of the Banda region the subducted slab dips steeply in the upper mantle and is deflected in the transition zone, in accord with the observed seismicity (Fig. 12a). This deflection, however, is not very well recovered by the inversion (Fig. 12e), and one should thus be cautious when interpreting from the images alone. The E–W-trending cross-section shows that the seismically fast slab dips rather gently, which is also in good agreement with seismicity in parts of the slab (Fig. 12b). Also here, the dip of the slab decreases abruptly in the transition zone. Although not resolved in detail, our images suggest that the slab beneath Banda forms a spoon-shaped structure in accord with inferences from earthquake locations (Cardwell & Isacks 1978).

The structure of the slab beneath the Banda arc, summarized in Fig. 13, can be explained in the context of recent northward movement of the Australian continent. In the Miocene, the small islands along the present-day curved Banda arc were striking E–W. In the Pliocene, a dramatic event occurred where the Banda arc was twisted counter-clockwise due to a

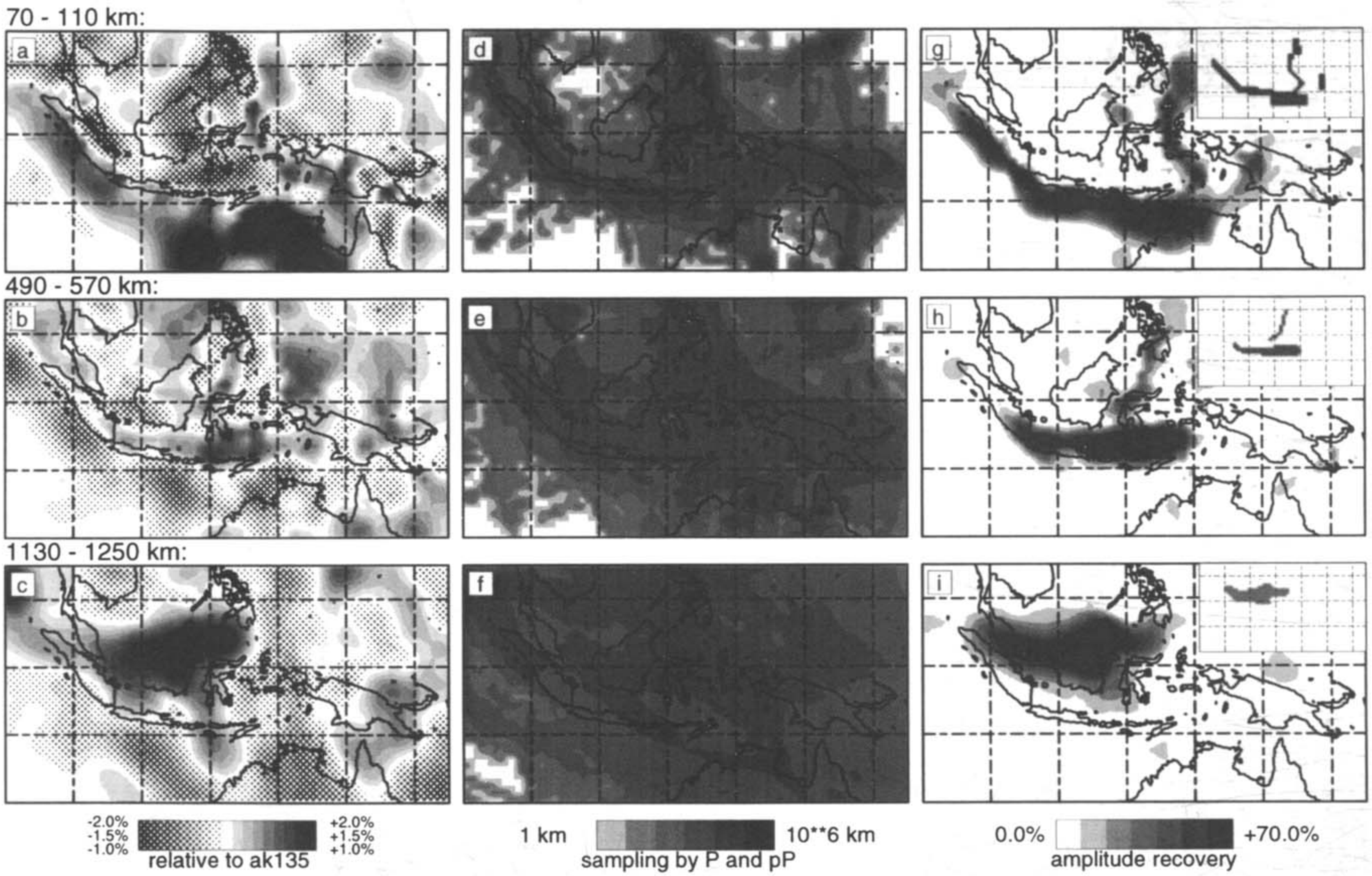

Figure 7. Results of tomographic inversions. (a)–(c) Solutions representing upper-mantle, transition-zone and lower-mantle structures with contour scales −2 to +2 per cent, −1.5 to +1.5 per cent and −1.0 to +1.0 per cent relative to ak135, respectively. (d)–(f) Sampling by *P*, *pP* and *pwP* rays at the corresponding depth intervals. (g)–(i) Recovery of a slab model designed from the inversion result in (a)–(c) plotted in percentage of amplitude of the input anomaly; see inset in the upper-right-hand corners for input at each depth interval. Velocity perturbations in the input model are set to 5, 4 and 3 per cent relative to ak135 for the slab in the upper mantle, transition zone and lower mantle, respectively, and zero elsewhere.

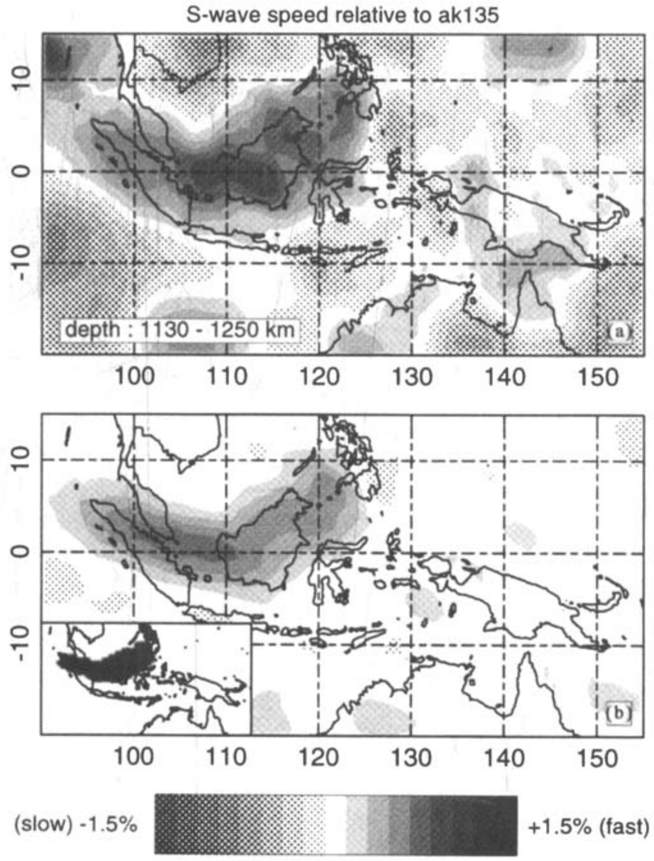

Figure 8. (a) A layer anomaly map representing lower-mantle structure from the inversion of *S* data. (b) Recovery of a slab model designed from the inversion result in (a); see inset in the lower-left-hand corner for input. Velocity perturbations in the input model are set to 2 per cent relative to ak135 in the slab model and zero elsewhere.

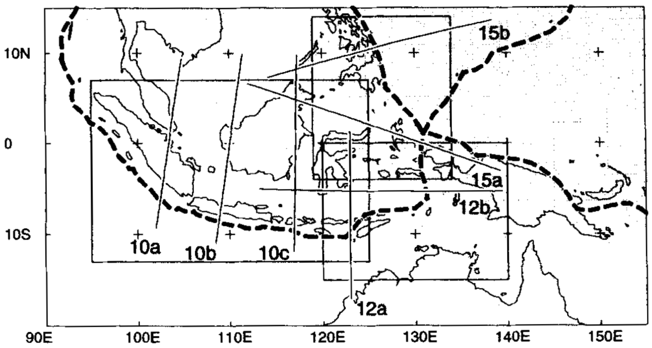

Figure 9. Subarea division to focus the presentation of tomographic images. Solid lines depict the positions of cross-sections; 10 (a)–(c), 12 (a)–(b) and 15 (a)–(b) are beneath the Sunda, Banda, and MCZ and Philippine Island regions, respectively.

combination of the northward drift of the Australian continent and the counter-clockwise rotation of New Guinea (Katili 1973). The deflection of the slab in the transition zone is likely to pre-date the rotation.

4.3 The MCZ and Philippine arc

The configuration of the Molucca Sea and Philippine Sea plates has been discussed by e.g. Silver & Moore (1978), Hamilton (1979), Cardwell *et al.* (1980) and Hall (1987). From seismicity, they inferred two oppositely dipping Benioff zones. With *P*-wave imaging Puspito *et al.* (1993) detected two opposing subducted slabs of the Molucca Sea plate and also the westward-subducted slab of the Philippine Sea plate beneath the Philippine Islands to the northeast of the MCZ. Our results are in good agreement with these observations, but suggest that the westward-subducting slab dips more steeply than the eastward one.

The image in Fig. 14(a) shows an offset between the top of the Molucca Sea and Philippine Sea plates at about 5°N, with the Molucca Sea plate located at the southwest corner of the Philippine Sea plate. The upper mantle beneath the MCZ and the Philippine arc are well sampled by seismic rays, and test inversions suggest that the major structures, including the observed offset between the Molucca Sea and Philippine Sea plates, are reliably imaged (Figs 14b and c). We present two arc-perpendicular vertical sections across the MCZ and southern Philippines (Figs 15a and b). The cross-section in Fig. 15(a) shows the two opposing subducted slabs of the Molucca Sea plate, with the dip of the westward-subducting slab steeper than that of the eastward-dipping slab. The image suggests that the westward-subducting slab penetrates into the lower mantle, but one must be aware of possible 3-D effects, since this intersects the deep part of the Java slab. In the west-dipping limb, seismicity is deeper than in the eastern seismic zone (see dots in Fig. 15a), which may imply that the westward subduction was either active longer or that it had a faster rate of subduction (Silver & Moore 1978). To the northeast of the Molucca Sea, the image reveals the subducted lithospheric slab that may be associated with the westward subduction of the Philippine Sea plate beneath the Philippines (Fig. 15b). Results of resolution tests suggest that the two opposing subducted slabs beneath the MCZ and the slab beneath the southern Philippines are resolved (Figs 15c–f). We simulated the inferred subhorizontal slab in the uppermost lower mantle beneath the reversed U-shape of the Molucca Sea plate (Fig. 15c). Its recovery (Fig. 15e) suggests that we have sufficient data coverage to resolve this intriguing and unexpected structure.

Our inferences from the images in general compare favourably with previous results. An important new observation is that the dips of the eastward- and westward-subducting slabs of the Molucca Sea plate are different. We postulate that this difference in dip angle is due to the shear caused by a combination of the westward thrust of the Pacific plate combined with movement on the left-lateral Sorong fault to the south of the Molucca Sea and viscous drag in the mantle. Hall (1987) reported that the westward shift of the Halmahera arc occurred in the Pleistocene. We summarize our preferred interpretation of the images using the block diagram given in Fig. 16, which is a slight modification of the geometry inferred by Cardwell *et al.* (1980).

5 DISCUSSION

Simultaneous inversion for regional and global-scale structure has successfully imaged major structures outside the study area and is likely to have minimized the mapping of distant structure into the study region. The inclusion of depth phases added significantly to the sampling and to focal-depth control, which improves the resolution of slab structure. The overall improvements of the resulting images are probably due to the

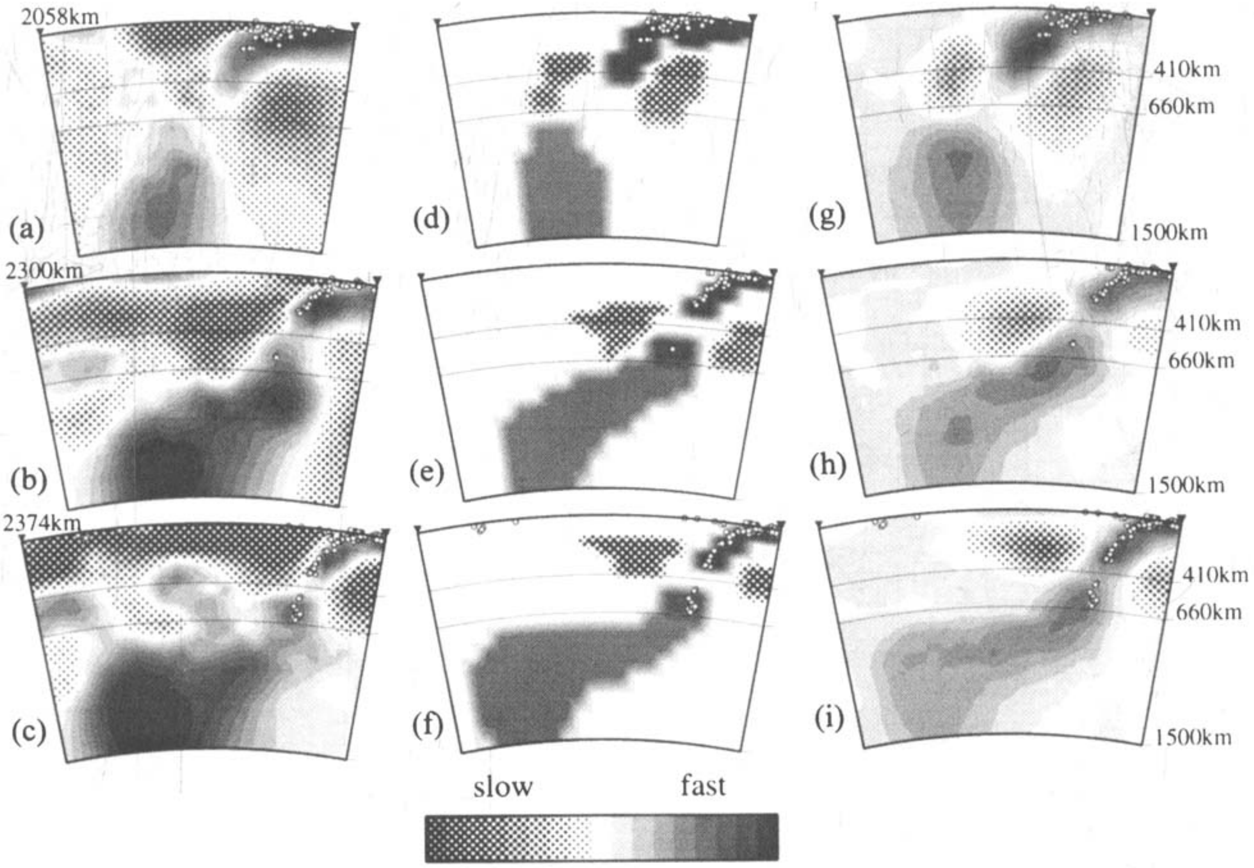

Figure 10. Vertical cross-sections of tomographic images across the Sunda arc. (a)–(c) Cross-sections beneath West Sunda (Sumatra), Central Sunda (Java) and East Sunda (between Flores and Java), respectively; contour scale: −1.0 to +1.0 per cent. Sections are plotted from the backarc in the north (left) to the forearc region in the south (right). Hereafter, open dots depict earthquake hypocentres of magnitude ≥5.5 on the Richter scale, projected from a distance of up to 50 km on both sides of the plane of section. (d)–(f) Model detached slabs synthesized from the slab structure displayed in (a)–(c); contour scale: −5.0 to +5.0 per cent. We added low-wave-speed anomalies just outside the model slab to assess the effect of the low-wave-speed anomalies observed in (a)–(c). In the slab and in the added low-wave-speed anomalies, *P*-wave velocity is 5, 4 and 3 per cent faster- and slower-than-average for the upper mantle, transition zone and lower mantle, respectively, and zero elsewhere. (g)–(i) Recovery of the model detached slabs in (d)–(f); contour scale: −5.0 to +5.0 per cent. Notice the loss of amplitude.

combination of the high quality of the reprocessed (EVB) data and the ak135 reference velocity model, the incorporation of depth phases, the simultaneous inversion for global structure and the use of gradient damping.

In a previous paper (INA1) we discussed in detail the structure of the slab beneath the Sunda arc and discussed how the complex slab structure could be related to the Tertiary evolution of southeastern Asia and the Indian Ocean region. In the previous section, we presented the results of resolution tests that substantiate the inferences in INA1, in particular the slab detachment beneath Sumatra and the kink in the slab beneath the eastern part of the Sunda arc. In INA1 we argued that the detachment beneath Sumatra may have been triggered by the rotation of the island in the Early Tertiary. The deep slab beneath the region as revealed by *P* and *S* data inversions (Figs 7c and 8a) is confirmed by the results of our inversions of *P* and *S* traveltime residuals for global structure shown in Figs 17(a) and (b). Our global images suggest that the deep structure beneath Indonesia forms the eastern end of a deep anomaly beneath southern Eurasia that is associated with the past subduction of the Mesozoic Tethys ocean floor (see also Van der Hilst, Widiyantoro & Engdahl 1997).

Near the boundary between the Sunda and Banda arcs, between Flores and Timor (Puspito & Shimazaki 1995), the images suggest an abrupt change in the depth of slab penetration into the mantle (see Fig. 4 in INA1). Beneath Banda the slab does not directly penetrate into the lower mantle but seems to deflect into the transition zone. The curved Banda arc can perhaps be explained in the context of continent–island-arc collision between the recent, about 5 Ma, northward movement of the Australian continent and the Banda arc. The collision may have caused the shortening of the upper plate in the convergence direction beneath the forearc and backarc basins over the area between the Timor trough and northern Banda (McCaffrey 1988). One of the most striking aspects of the Banda arc is the apparent counter-clockwise rotation of almost 180°. The rotation may have formed the narrow deep region in the Banda Sea, named the Weber Deep, which is assumed to be oceanic crust trapped by the surrounding younger arcs (Katili 1975). The curious high-wave-speed anomaly in the uppermost lower mantle (Fig. 12b) may represent excess slab materials that have resulted from the distortion of the deflected slab. Cardwell & Isacks (1978) interpret the subduction zone to the north of the Banda Sea as not being a continuation of that along the southern and eastern parts of the arc. Our inversions cannot resolve such

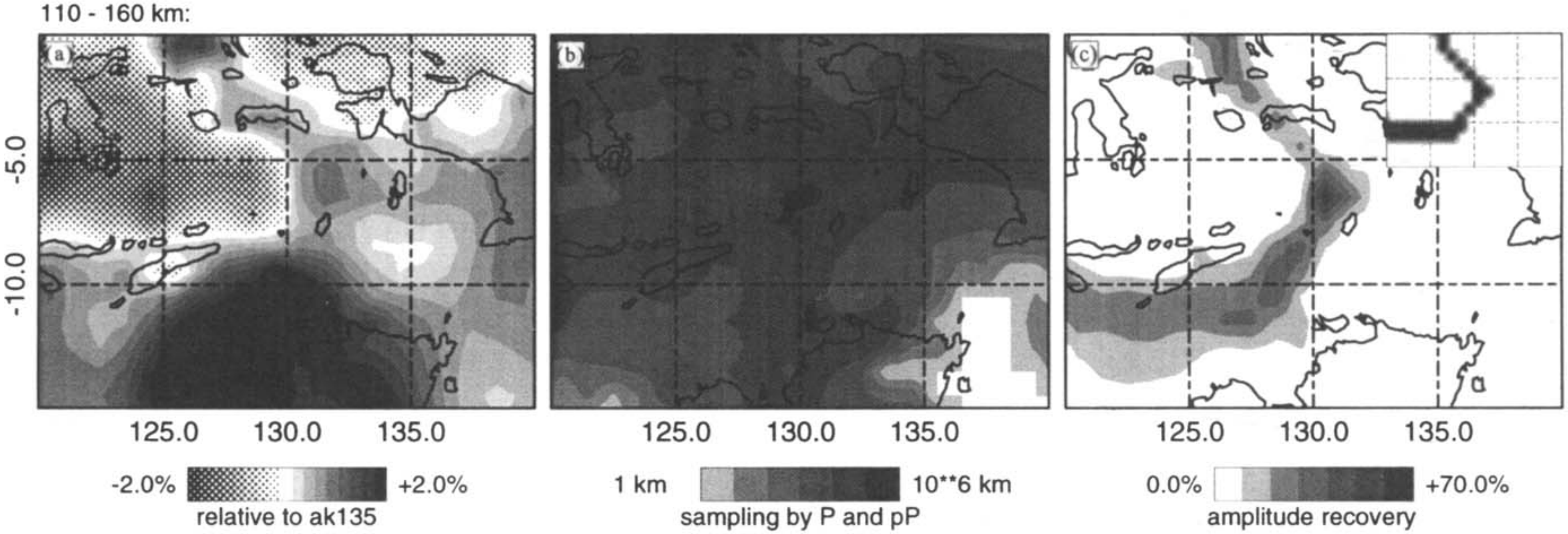

Figure 11. Close-up of inversion results representing the structure in the upper mantle beneath the Banda arc. (a) *P*-wave velocity relative to ak135. (b) Sampling by *P*, *pP* and *pwP* rays. (c) Recovery of a slab model designed from the inversion result in (a) plotted in percentage of amplitude of the input anomaly; see inset in the upper-right-hand corner for input. Velocity perturbation in the model slab is set to 5 per cent relative to ak135 and zero elsewhere.

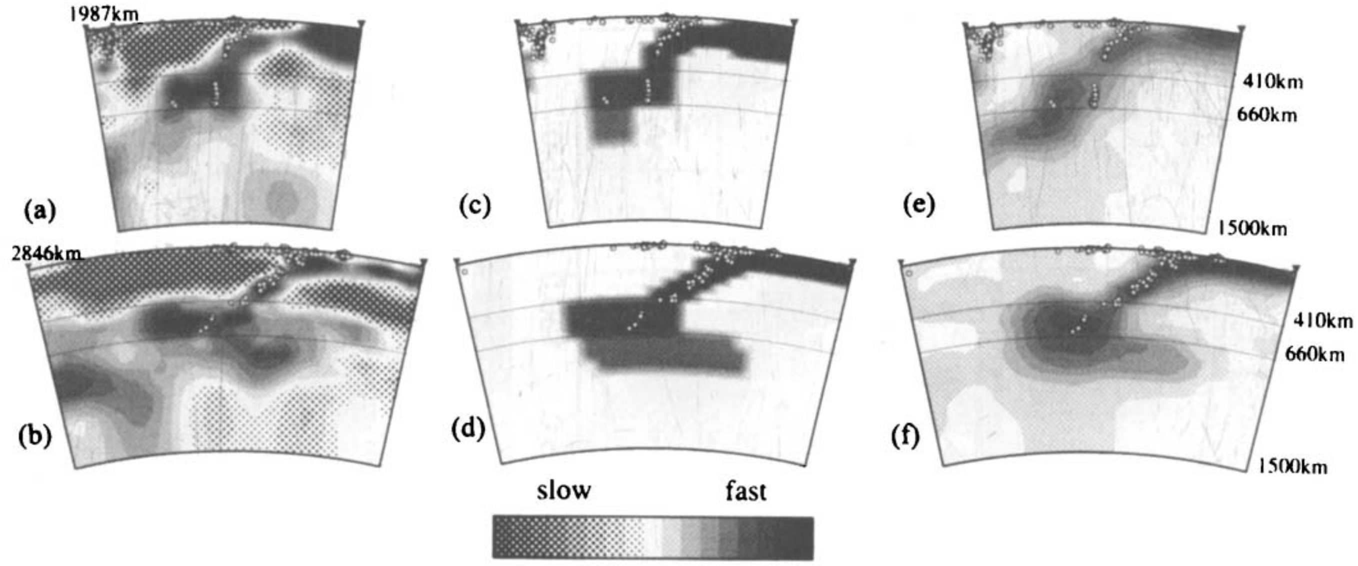

Figure 12. Vertical cross-sections of tomographic images across the Banda arc. (a) and (b) Cross-sections plotted from the inner arc in the north (left) to the outer-arc region in the south (right) and from the inner arc in the west (left) to the outer-arc region in the east (right), respectively; contour scale: −1.0 to +1.0 per cent. (c) and (d) Model slabs synthesized from the slab structure displayed in (a) and (b); contour scale: −5.0 to +5.0 per cent. In the slab, *P*-wave velocity is 5, 4 and 3 per cent faster than average for the upper mantle, transition zone and lower mantle, respectively, and zero elsewhere. (e) and (f) Recovery of the model slabs in (c) and (d); contour scale: −5.0 to +5.0 per cent. Notice the loss of amplitude.

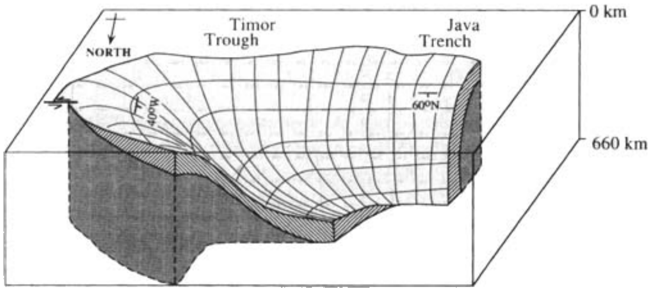

Figure 13. Block diagram illustrating the geometry of the subducted lithospheric slab beneath the Banda arc [modified from Cardwell & Isacks (1978) based on the tomographic images]. Modifications were made to show clearly that the structure beneath Banda forms a spoon-shaped feature of the descending slab with a left-lateral fault in the eastern part of the Banda arc as inferred from seismicity (e.g. Cardwell & Isacks 1978). Notice the existence of the southward-subducted slab beneath the northern part of Banda.

detail. The complete exploration of the lateral variation in the shape of the subducted slab (e.g. Figs 12a and b) and inferences from seismicity suggest that the large-scale structure of the slab in the upper mantle and transition zone beneath Banda forms a spoon-shaped feature (Fig. 13).

The structure of the subducted slab beneath the Molucca collision zone is more complex than beneath other convergent margins. The MCZ is underlain by two oppositely dipping slabs associated with the subducted Molucca Sea plate. The westward thrust of the Pacific plate, combined with the large left-lateral movement of the Sorong fault to the south of the Molucca Sea, may have shifted the Molucca Sea plate and its surrounding microplates towards the Eurasian continent. This shift may have caused the offset between the Philippine Sea and Molucca Sea plates (Fig. 14a) as well as the observed different dips of the opposing subducted slabs (see Fig. 15a). Puspito *et al.* (1993) discussed the westward-dipping slab beneath the MCZ penetrating into the lower mantle. Due to the complex geological setting in Indonesia, however, we must be cautious when interpreting the origin of deep anomalies beneath the region. Not all deep anomalies can be traced back unambiguously to slab structure in the shallower mantle; in complex regions the use of 2-D cross-sections can be misleading. We argue that the deep high-wave-speed anomaly west of the MCZ mostly represents the deep Indo–Australian slab subducted towards the north along the Sunda arc (Fig. 10c). Our argument is based both on a careful examination of the 3-D model and on the size of the plate. The Molucca Sea plate is relatively small and is unlikely to have formed such a large, deep anomaly. Furthermore, the long subduction history of the Indo–Australian plate supports our argument, whereas the subduction of the Molucca Sea plate is only recent. A confusing feature, which is within our resolution, is the subhorizontal anomaly in the uppermost lower mantle beneath the Molucca Sea plate (Fig. 15a). We do not know its origin. One may speculate that it may be a remnant slab of past subduction of the Pacific plate. To the northeast of the Molucca Sea, the image (Fig. 15b) shows that the subducted lithospheric slab associated with the westward-subducting Philippine Sea plate seems also to penetrate into the uppermost lower mantle beneath the southern Philippine arc. Based on inferences from the complete images and from the seismicity, however, we prefer to interpret the shallow part of the slab as being associated with the subducted Philippine Sea plate, while the deeper part may correspond to the westward-dipping slab of the Molucca Sea plate. This preferred interpretation suggests that the deeper part of the westward-dipping slab of the Molucca Sea plate extends to the north up to the mantle beneath the southern Philippines. The interpretation of the northward extension of the deep slab is supported by the corresponding deep seismicity (Fig. 5b) and the fast *P*-wave-

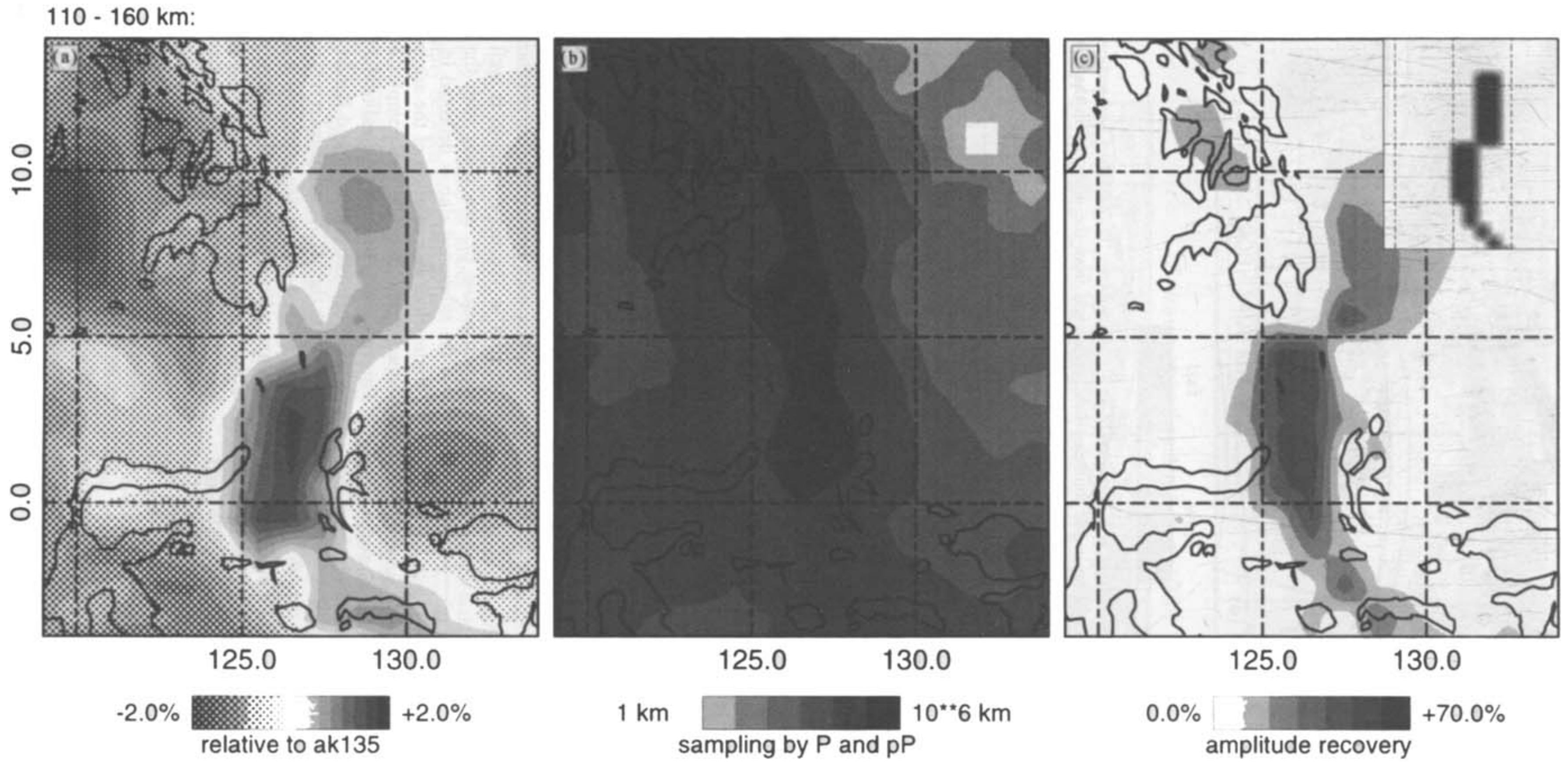

Figure 14. Close-up of inversion results representing the structure in the upper mantle beneath the MCZ and Philippine arc. (a) *P*-wave velocity relative to ak135. (b) Sampling by *P*, *pP* and *pwP* rays. (c) Recovery of a slab model designed from the inversion result in (a) plotted in percentage of amplitude of the input anomaly; see inset in the upper-right-hand corner for input. Velocity perturbation in the model slab is set to 5 per cent relative to ak135 and zero elsewhere.

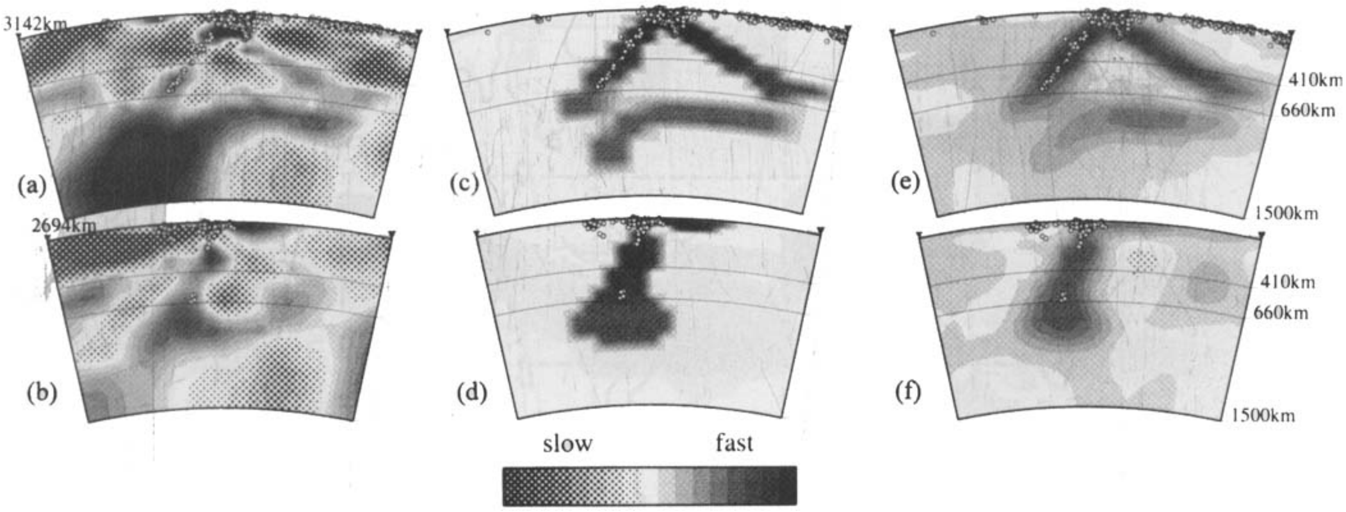

Figure 15. Vertical cross-sections of tomographic images across the MCZ and Philippine arc. (a) and (b) Cross-sections plotted from the inner arc in the northwest–west (left) to the outer-arc region in the southeast–east (right) and from the inner arc in the southwest–west (left) to the outer-arc region in the northeast–east (right), respectively; contour scale: -1.0 to $+1.0$ per cent. (c) and (d). Model slabs synthesized from the slab structure displayed in (a) and (b); contour scale: -5.0 to $+5.0$ per cent. In the slab, *P*-wave velocity is 5, 4 and 3 per cent faster than average for the upper mantle, transition zone and lower mantle, respectively, and zero elsewhere. (e) and (f) Recovery of the model slabs in (c) and (d); contour scale: -5.0 to $+5.0$ per cent. Notice the loss of amplitude.

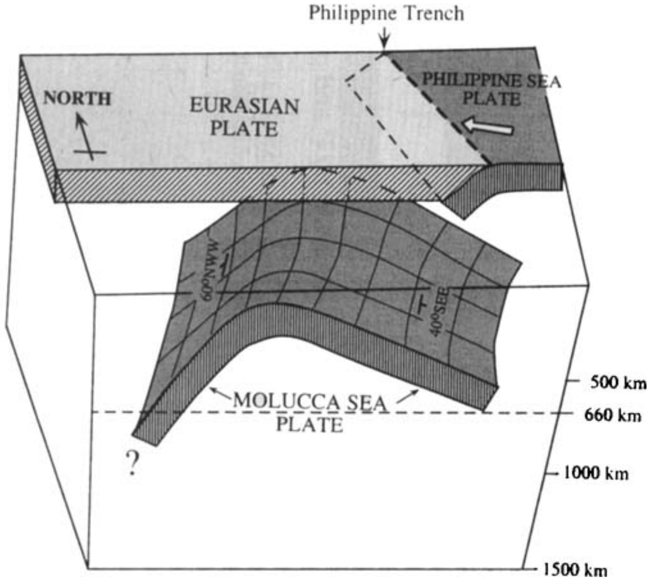

Figure 16. Configuration of the Molucca Sea and Philippine Sea plates [modified from Cardwell *et al.* (1980), based on the tomographic images]. An important modification is that the westward subduction of the Molucca Sea plate is steeper than the eastward subduction, that is ~60° and ~40°, respectively. See text for discussion.

speed slab trending almost N–S from the Philippines to north Sulawesi (Fig. 7b). It is also in accord with the present strike of the Sangihe and Halmahera arcs, that is NNE–SSW, and with the WNW direction of the Pacific plate motion.

6 CONCLUDING REMARKS

The new tomographic images reveal the mantle structure beneath Indonesia in more detail than previous studies. The improvements are likely to be due to the combination of the use of better data (extensively processed EVB data instead of ISC), the use of the ak135 reference velocity model, the inclusion of a global inversion in the regional study, the use of depth phases and the use of gradient damping. The results of resolution tests suggest that the large-scale slab structure beneath the Indonesian archipelago is resolved by either *P* or *S* data. In spite of relatively noisy data, the results of *S* data inversion are in general in good agreement with those from *P* data.

In the top of the lower mantle beneath the eastern part of the Sunda arc, the subducted slab forms a kink, which gradually disappears further west. Beneath Sumatra the image suggests that the slab is detached in the transition zone. The interpreted 'necking' of the slab beneath Java coincides with the pronounced existing seismic gap. In a previous paper (INA1) we related this complex slab structure to the Tertiary evolution of southeastern Asia and the Indian Ocean region.

Further east, beneath the curved Banda arc, the twisting of the slab in the upper mantle is well imaged. The vertical section across the arc, along with the anomaly maps, show that the subducted slab is deflected in the transition zone. A counter-clockwise rotation of the arc has resulted in a spoon-shaped structure of the slab complex beneath the Banda Sea. This rotation is probably related to the Pliocene continent–arc collision between Australia and Banda.

Beneath the MCZ the images reveal two opposing subducted slabs of the Molucca Sea plate, which are related to the active arc–arc collision between Halmahera and Sangihe. The dips of the two slab segments are significantly different, which may be due to the westward shift of the slab complex in a viscous mantle. Although the wave-speed anomaly associated with the westward-dipping subduction seems to continue into the uppermost part of the lower mantle, this deep structure is more likely to be associated with the deep subduction of the Indo–Australia plate along the Sunda arc. The use of 2-D cross-sections in such complex structures can thus be misleading. The westward-dipping slab beneath the MCZ may extend further north to beneath the southern Philippines.

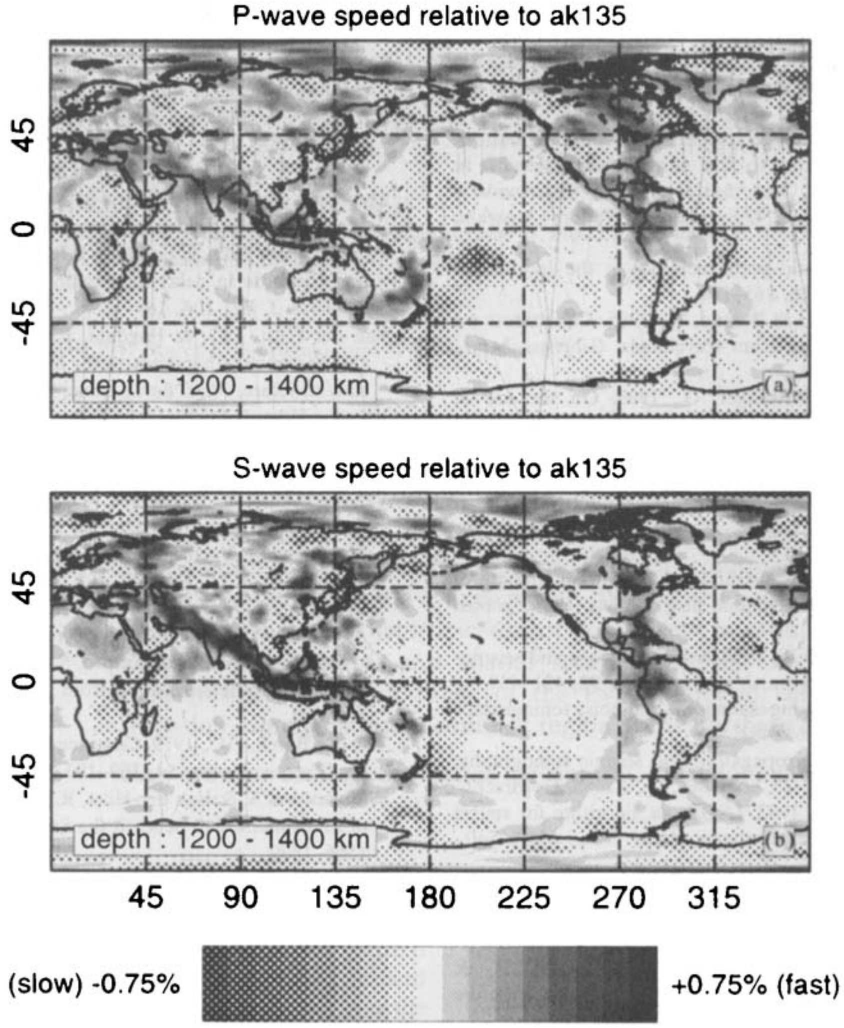

Figure 17. (a) A layer anomaly map in the lower mantle from an inversion of *P* data for global structure. We used more than 7.0×10^6 data on the inversion and fine parametrization with a horizontal cell size of $2^\circ \times 2^\circ$ for the whole globe (Van der Hilst *et al.* 1997). (b) The same as (a), but inferred from *S* data (Widiyantoro, Kennett & Van der Hilst, in preparation). Notice the long, positive anomaly stretching from the Mediterranean to the Indonesian region.

Anomaly maps in the upper mantle reveal the offset of the Molucca Sea and Philippine Sea plates at about 5°N, which may indicate the boundary between these two plates.

ACKNOWLEDGMENTS

We are grateful to B. L. N. Kennett for useful discussions and reviews, E. R. Engdahl for early versions of the hypocentre and phase data set, and G. Nolet for his LSQR inversion code. We thank J. Weekes for the excellent picking of phase arrivals in the SKIPPY records used in this study and C. Krayshek for producing the final drafts of Figs 13 and 16. This manuscript benefited from the reviews of two anonymous referees.

REFERENCES

Bullen, K.E. & Bolt, B.A., 1985. Seismic ray in a spherically stratified Earth model, in *An Introduction to the Theory of Seismology,* pp. 153–184, Cambridge University Press, Cambridge.

Cardwell, R.K. & Isacks, B.L., 1978. Geometry of the subducted lithosphere beneath the Banda Sea in eastern Indonesia from seismicity and fault plane solutions, *J. geophys. Res.,* **83,** 2825–2838.

Cardwell, R.K., Isacks, B.L. & Karig, D.E., 1980. The spatial distribution of earthquakes, focal mechanism solutions and plate boundaries in the Philippine and northeastern Indonesia Islands, *Am. geophys. Un., Geophys. Monogr.,* **23,** 1–35.

DeMets, C., Gordon, R.G., Argus, D.F. & Stein, S., 1990. Current plate motions, *Geophys. J. Int.,* **101,** 425–478.

Engdahl, E.R., van der Hilst, R.D. & Buland, R., 1997. Global teleseismic earthquake relocation with improved travel times and procedures for depth determination, *Bull. seism. Soc. Am.,* submitted.

Fukao, Y., Obayashi, M., Inoue, H. & Nenbai, M., 1992. Subducting slabs stagnant in the mantle transition zone, *J. geophys. Res.,* **97,** 4809–4822.

Gubbins, D., 1990. Refining the locations, in *Seismology and Plate Tectonics,* pp. 119–122, Cambridge University Press, Cambridge.

Hall, R., 1987. Plate boundary evolution in the Halmahera region, Indonesia, *Tectonophysics,* **144,** 337–352.

Hamilton, W., 1979. Tectonics of the Indonesian region, *USGS Prof. Paper,* **1078.**

Humphreys, E. & Clayton, R.W., 1988. Adaption of back projection tomography to seismic travel time problems, *J. geophys. Res.*, **93,** 1073–1085.

Inoue, H., Fukao, Y., Tanabe, K. & Ogata, Y., 1990. Whole mantle P-wave travel time tomography, *Phys. Earth planet Inter.*, **59,** 294–328.

Katili, J.A., 1973. On fitting certain geological and geophysical features of the Indonesian Island arcs to the new global tectonics, in *The Western Pacific: Island Arcs, Marginal Seas, Geochemistry,* pp. 287–305, ed. P.J. Coleman, University of Western Australia Press, Perth.

Katili, J.A., 1975. Volcanism and plate tectonics in the Indonesian Island arcs, *Tectonophysics,* **26,** 165–188.

Kennett, B.L.N., Engdahl, E.R. & Buland, R., 1995. Constraints on seismic velocities in the Earth from traveltimes, *Geophys. J. Int.*, **122,** 108–124.

Léveque, J.J., Rivera, L. & Wittlinger, G., 1993. On the use of the checker-board test to assess the resolution of tomographic inversions, *Geophys. J. Int.*, **115,** 313–318.

McCaffrey, R., 1988. Active tectonics of the Sunda and Banda arcs, *J. geophys. Res.*, **93,** 15 163–15 182.

Minster, J.B. & Jordan, T.H., 1978. Present-day plate motions, *J. geophys. Res.*, **83,** 5331–5354.

Moresi, L. & Gurnis, M., 1996. Constraints on the lateral strength of slabs from three-dimensional dynamic flow models, *Earth planet. Sci. Lett.*, **138,** 15–28.

Newcomb, K.R. & McCann, W.R., 1987. Seismic history and seismotectonics of the Sunda arc region, *J. geophys. Res.*, **92,** 421–439.

Nolet, G., 1985. Solving or resolving inadequate and noisy tomographic system, *J. Comp. Phys.*, **61,** 463–482.

Nolet, G., 1987. Seismic wave propagation and seismic tomography, in *Seismic Tomography*, pp. 1–23, ed. Nolet, G., Reidel, Dordrecht.

Paige, C.C. & Saunders, M.A., 1982. LSQR: an algorithm for sparse linear equations and sparse least squares, *ACM Trans. Math. Soft.*, **8,** 43–71; 195–209.

Puspito, N.T. & Shimazaki, K., 1995. Mantle structure and seismotectonics of the Sunda and Banda arcs, *Tectonophysics,* **251,** 215–228.

Puspito, N.T., Yamanaka, Y., Miyatake, T., Shimazaki, K. & Hirahara, K., 1993. Three-dimensional P-wave velocity structure beneath the Indonesian region, *Tectonophysics,* **220,** 175–192.

Ranken, B., Cardwell, R.K. & Karig, D.E., 1984. Kinematics of the Philippine Sea plate, *Tectonics,* **3,** 555–575.

Silver, E.A. & Moore, J.C., 1978. The Molucca Sea collision zone, Indonesia, *J. geophys. Res.*, **83,** 1681–1691.

Spakman, W. & Nolet, G., 1988. Imaging algorithms, accuracy and resolution in delay time tomography, in *Mathematical Geophysics: a Survey of Recent Developments in Seismology and Geodynamics,* pp. 155–188, eds Vlaar, N.J., Nolet, G., Wortel, M.J.R. & Cloetingh, S.A.P.L., Reidel, Dordrecht.

Tregoning, P. *et al.*, 1994. First geodetic measurement of convergence across the Java Trench, *Geophys. Res. Lett.*, **21,** 2135–2138.

Van der Hilst, R.D. & Engdahl, E.R., 1991. On ISC PP and pP data and their use in delay-time tomography of the Caribbean region, *Geophys. J. Int.*, **106,** 169–188.

Van der Hilst, R.D. & Engdahl, E.R., 1992. Step-wise relocation of ISC earthquake hypocentres for linearized tomographic imaging of slab structure, *Phys. Earth planet Inter.*, **75,** 39–53.

Van der Hilst, R.D., Engdahl, E.R., Spakman, W. & Nolet, G., 1991. Tomographic imaging of subducted lithosphere below northwest Pacific Island arcs, *Nature,* **353,** 37–43.

Van der Hilst, R.D., Engdahl, E.R. & Spakman, W., 1993. Tomographic inversion of P and pP data for aspherical mantle structure below the northwest Pacific region, *Geophys. J. Int.*, **115,** 264–302.

Van der Hilst, R.D., Kennett, B.L.N., Christie, D. & Grant, J., 1994. Project *Skippy* explores the lithosphere and mantle beneath Australia, *EOS, Trans. Am. geophys. Un.*, **75,** 177; 180–181.

Van der Hilst, R.D., Widiyantoro, S. & Engdahl, E.R., 1997. Evidence for deep mantle circulation from global tomography, *Nature,* **386,** 578–584.

Von der Borch, C.C., 1979. Continent–island arc collision in the Banda arc, *Tectonophysics,* **54,** 169–193.

Widiyantoro, S. & Van der Hilst, R.D., 1996. Structure and evolution of lithospheric slab beneath the Sunda arc, Indonesia, *Science,* **271,** 1566–1570.

Wortel, M.J.R. & Vlaar, N.J., 1988. Subduction zone seismicity and the thermomechanical evolution of downgoing lithosphere, *Pageoph.*, **128,** 625–659.

Zielhuis, A. & Nolet, G., 1994. Deep seismic expression of an ancient plate boundary in Europe, *Science,* **265,** 79–81.

Zielhuis, A. & Van der Hilst, R.D., 1996. Upper mantle shear velocity beneath eastern Australia from inversion of waveforms from SKIPPY portable arrays, *Geophys. J. Int.*, **127,** 1–16.